CHEMISTRY OF MATERIALS

pubs.acs.org/cm

Article

High Conductivities of Disordered P3HT Films by an Electrochemical Doping Strategy

David Neusser, Claudia Malacrida, Michal Kern, Yannic M. Gross, Joris van Slageren, and Sabine Ludwigs*

Cite This: *Chem. Mater.* 2020, 32, 6003−6013

Read Online

ACCESS | Metrics & More | Article Recommendations | Supporting Information

ABSTRACT: In this work, we demonstrate that high solid-state conductivities of simply spin-coated poly(3-hexylthiophene) (P3HT) films can be obtained by means of an *ex situ* electrochemical doping strategy using 4-line electrodes. With increasing electrochemical doping potential, we find an increase in conductivity over 6 orders of magnitude, giving a maximum conductivity up to 224 S cm^{-1} with maximum hole densities of 10^{21} holes per cm^3. Most intriguingly, highly conducting states are achieved over a very broad potential range from 0.4 to 0.8 V *versus* Fc/Fc^+ in the doped state. The experiments are complemented by UV−vis−NIR absorption and electron paramagnetic resonance spectroscopy in the solid state as well as with *in situ* electrochemical measurements which confirm that the electrochemically generated doped species can be successfully transferred into the solid state. Our results suggest that for reaching high conducting states, P3HT has to be present in different redox states and that the plateau conductivity region should arise from the coexistence of overlapping polaron and bipolaron states. Comparisons to films of regiorandom P3HT and pure redox polymer systems based on diphenyl-3,3′-bicarbazyl are further presented, which highlight the role of mixed valence states in conducting polymers. Last but not least, the highly conducting films are simply spin-coated and therefore rather disordered, adding new aspects to the discussion whether high crystallinity is a prerequisite for achieving high conductivities in conjugated polymers.

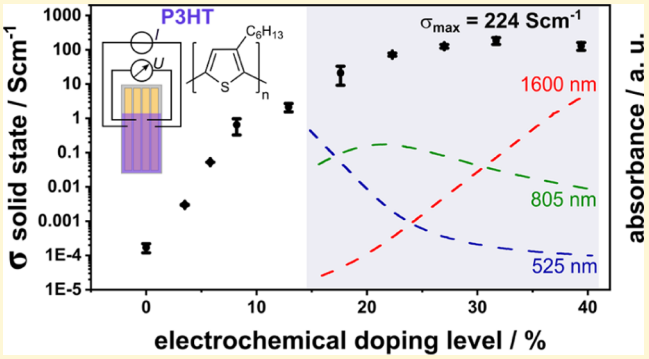

1. INTRODUCTION

Conducting polymers (CPs) feature a unique set of properties such as low weight, processability from solution, and intrinsic electronic conductivity upon doping, explaining their successful integration in numerous applications in the field of organic electronics and electrochemical devices in the last years.[1−3] Depending on their chemical nature, CPs can be divided into conjugated and redox polymers.[4] In redox polymers, charge transport is governed by pure hopping transport between localized redox units that are in different oxidation states, following a well-accepted mixed valence conductivity model.[5−8] Conjugated polymers on the other hand are based on long π-conjugated backbones that allow inter- and intrachain transport between the chains. Charge carriers go along with a geometrical deformation, delocalized over multiple repeating units and are hence usually referred to as polaron and bipolaron species.[8−11] The existence of mixed conductivity mechanisms also in conjugated polymers, that is, treating the polymer as molecular redox systems has been, for example, proposed in the work of Heinze and co-workers.[12−15]

Poly(3-hexylthiophene) (P3HT) is one of the most studied conjugated polymers and is often considered to be the workhorse in the field of organic electronics devices because of a variety of realized applications.[2] Regioregular P3HT with high regioregularity can be assigned to the group of semicrystalline polymers, which—depending on the processing conditions—can be obtained in morphologies ranging from mainly amorphous films with short-range order to highly crystalline films with large-scale well-oriented domains. Techniques such as mechanical rubbing[16−18] and controlled crystallization in solvent vapor atmospheres[19] have been used for increasing crystallinity and improving orientation of the chains with respect to substrates in preferentially face-on and edge-on orientations to measure anisotropic charge transport.[17,18,20]

The conductivity of pristine neutral CPs can be increased over several orders of magnitude by means of chemical or electrochemical doping. Regarding chemical doping approaches of polymer films, the dopant can either be directly

Received: March 26, 2020
Revised: June 29, 2020
Published: July 10, 2020

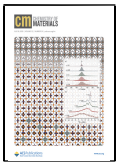

https://dx.doi.org/10.1021/acs.chemmater.0c01293
Chem. Mater. 2020, 32, 6003−6013

Scheme 1. Schematic Overview of an Electrochemical Bulk Doping Process in a Three-Electrode Geometry; This Doping Technique can be Coupled with *In Situ* Conductance and UV−Vis−NIR Spectroscopy Performed in Liquid Electrolyte (*In Situ*, Top) Inside the Electrochemical Cell and Further Allows for *Ex Situ* Measurements of Solid-State Bulk Conductivities in Combination with Spectroscopic Tools after Removing the Doped Films from the Electrochemical Cell (*Ex Situ*, Bottom)

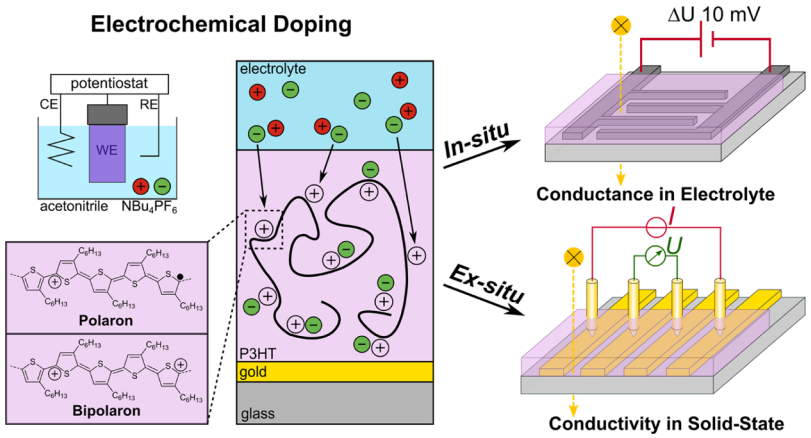

mixed with the polymer in solution and then deposited as blend[21] or sequentially added to as-cast films either through the vapor phase or by using dip- or spin-doping approaches.[22−24] The advantage of the latter approach is that morphology optimization in terms of improving order and orientation can be conducted to the films before they are exposed to the dopant.[25,26]

Because of matching energy levels, chemical redox dopants like $FeCl_3$,[27] 2,3,5,6-tetrafluoro-7,7,8,8-tetracyanoquinodimethane (F_4TCNQ),[28] and dodecaborane clusters[29] were presented as strong and efficient dopants for P3HT which has the highest occupied molecular orbital (HOMO) energy of −5.1 eV[30] (when determined from an electrochemical oxidation onset of ∼0 V *vs* Fc/Fc^+, using the correction factor of 5.1 eV[31]). Müller and co-workers provided a systematic conductivity comparison on using different solvents for spin-coating of P3HT films which were subsequently vapor-doped with F_4TCNQ.[32] These results strongly suggest that high order in terms of crystallinity is necessary to obtain high conductivities.[16,30,32] However, alternative theories proposed by Zozoulenko and co-workers hypothesize that only efficient $\pi-\pi$ aggregation with a network of percolation paths seems to be essential for high electric performance and can outweigh the importance of perfect long-range crystalline order.[33−35]

An outstanding feature of electrochemical doping is the possibility for precisely adjusting the redox doping potentials and therefore the induced doping levels and charge carrier densities in the polymer.[36−38] Electrochemical measurements are typically performed in three-electrode setups and can be performed either statically or dynamically, providing the additional advantage of reversible doping and dedoping. The influence of the used supporting electrolyte, most commonly $TBAPF_6$, is not to be underestimated because the doping process is accompanied by the incorporation of counterions from the electrolyte into the polymer film to stabilize the induced charge carriers on the conjugated moieties. Only if the counterions are able to penetrate the bulk polymer film and remain inside the film, acceptable stability of the doped states can be realized.[12,37]

While fundamental electrochemistry of CPs is a mature field in the electrochemical literature, only recently its important experimental value has started to impact the polymer electronics and materials science communities. New applications like organic electrochemical transistors (OECTs)[39,40] and thermoelectric devices are nowadays hot topics in terms of energy conversion.[41−43] Electrochemical doping represents the fundamental mechanism in OECTs,[44] where the charge density inside the semiconductor layer is varied to tune the strength of the drain currents occurring in the transistor channel.[39,40,45,46]

It is essential to differentiate between a field effect-based charging (accumulation of charge carriers at the semiconductor−electrolyte interface) and an electrochemical doping of the bulk material with diffusion of ions into the semiconductor film. We refer to the literature which discusses differences in the working principles for devices built from P3HT.[37,47,48] Berggren *et al.* used the OECT configuration to monitor thermoelectric performance of poly(3,4-ethylenedioxythiophene) as function of the doping level.[49,50]

In this study, we present a new approach to fine-tuning solid-state conductivities by *ex situ* electrochemical bulk doping, which goes beyond classical *in situ* electrochemical approaches.[5,51] *Ex situ* in this context means semiconducting films are first electrochemically doped, then taken out of the electrochemical cell, dried under inert conditions, and measured with 4-line probe conductivity measurements.

Maximum conductivities of regioregular P3HT films of as high as 224 S cm^{-1} are obtained in the solid state. Most importantly, the highly conducting state is achieved over a broad potential range, namely, from 0.4 to 0.8 V (*vs* Fc/Fc^+). Intriguingly, the P3HT films are simply spin-coated, that means, have not been further ordered or oriented. Comparisons to regiorandom P3HT films with conductivities up to 10 S cm^{-1} are included to discuss the role of disorder in the films.

This manuscript is organized as follows: In the first step, we explore the electrochemical doping behavior employing cyclic voltammetry (CV) coupled with *in situ* conductance and *in situ* UV−vis−NIR spectroscopy in the electrolyte (see Scheme 1, top). This set of experiments allows us to systematically identify regions of highest conductivities and additionally assign the generated redox species which are responsible for the charge transport.

We then present our new 4-band electrode design which on the one hand allows to perform electrochemical doping in the

https://dx.doi.org/10.1021/acs.chemmater.0c01293
Chem. Mater. 2020, 32, 6003−6013

electrolyte and on the other hand enables obtaining reliable conductivities in the solid state after doping by 4-line conductivity measurements (see Scheme 1, bottom). The conductivity measurements are complemented with UV−vis−NIR and electron paramagnetic resonance (EPR) spectroscopy. Our experiments show that species that are generated *in situ* in the electrochemical measurements can be fully transferred to the solid state and suggest that the presence of P3HT in different redox states is needed for highly conducting states.

The role of mixed charge carrier species for achieving high conductivities is discussed by a comparison to electrochemically cross-linked vinyl polymer films containing redox-active bis(phenylcarbazole) (BCbz) moieties which are prone to mixed valence conductivity.[8,52]

2. RESULTS AND DISCUSSION

2.1. *In Situ* CV Studies of P3HT Films. First, a basic electrochemical characterization was performed to reveal the nature of the charge carriers upon electrochemical doping in the oxidative region from −0.2 up to 0.9 V. We refrained from exploring higher doping potentials to avoid irreversible side reactions in the polymer film which can occur at extreme oxidation potentials.[53]

The CV is, as typical for conjugated polymer films, quite broad without distinct peaks (see Figure 1a) which can be attributed to the oxidation of multiple overlapping redox states.[12,54] The oxidation onset is around 0 V which results in a HOMO level of −5.1 eV.[30] Because of the absence of a strong redox wave between 0.11 and 0.13 V, the spin-coated P3HT films can be regarded as mainly disordered.[30] The nearly complete absence of an absorption shoulder at 610 nm, which is characteristic for a vibrational fine structure of aggregated and crystalline P3HT films,[55,56] further indicates that our films can be specified as rather disordered. The low crystallinity of our films becomes even more clear when comparing the CV and spectroelectrochemistry data to results of completely amorphous films of regiorandom P3HT (see Figure S2).

The *in situ* spectroscopy data in Figure 1b provide a deeper insight into the conduction mechanism by giving information about the generated charged species when increasing the potential. In the case of P3HT, three characteristic absorption spectra can be identified: a neutral, a first oxidation state, and a second oxidation state. With respect to well-accepted literature, these spectra can be assigned to the neutral species, polarons, and bipolarons.[51,57,58] The neutral P3HT film shows a distinct absorption band at 525 nm, and no further signals at higher wavelengths (inset in Figure 1).

Above the oxidation onset of 0 V, the absorption band of the neutral species starts to decrease in favor of an intermediate band at 805 nm. A broad absorption in the wavelength region of 1600 nm starts to develop above 0.3 V, when the band at 805 nm has already reached substantial intensity. The 805 nm band reaches its maximum at an oxidation potential of 0.5 V and starts to decrease again when going to potentials beyond 0.5 V. In contrast, the broad signal at 1600 nm constantly increases up to the maximum oxidation potential of 0.86 V. In agreement with the traditional literature, the band at 805 nm can be assigned mainly to polaronic species, whereas the broad absorption above 1600 nm is rather correlated to bipolarons at high doping levels.[51,57,59] Comparison with *in situ* EPR spectroelectrochemistry data supports this assignment.[51] Recent literature by Zozoulenko *et al.* uses density functional

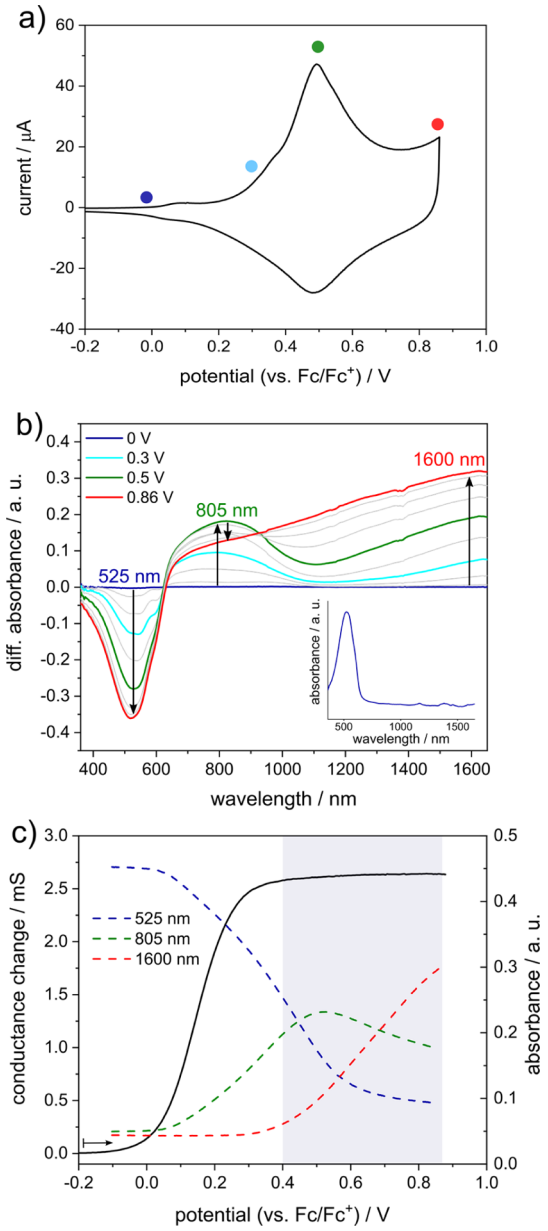

Figure 1. *In situ* electrochemical studies of a P3HT film spin-coated from $CHCl_3$ solution. (a) CV measured in 0.1 M $TBAPF_6$/MeCN at 20 mV s^{-1} on an interdigitated Pt electrode, (b) correlating *in situ* UV−vis−NIR spectra at the given potentials. The neutral spectrum of P3HT is inserted in the bottom right corner. (c) Changes of the *in situ* conductance measured in 0.1 M $TBAPF_6$/MeCN at 10 mV s^{-1} on an interdigitated Pt electrode (forward scan) and evolution of the absorption maxima at 525, 805, and 1600 nm corresponding to the characteristic species in the forward scan from (b). The complete *in situ* spectroelectrochemistry and *in situ* conductance data are given in the Supporting Information.

theory (DFT) calculations to give evidence that both polarons and bipolarons give rise to two absorption maxima, meaning polarons also contribute to a certain degree to the absorption at wavelengths above 1600 nm and bipolarons absorb also to some extent around 800 nm.[11]

Especially in the case of oligomeric species, literature further discusses the existence of σ-dimers, π-dimers, and polaron pairs as alternative charged species.[38,60−62] Regarding our obtained data, we do not see clear evidence for the existence of other

https://dx.doi.org/10.1021/acs.chemmater.0c01293
Chem. Mater. 2020, 32, 6003−6013

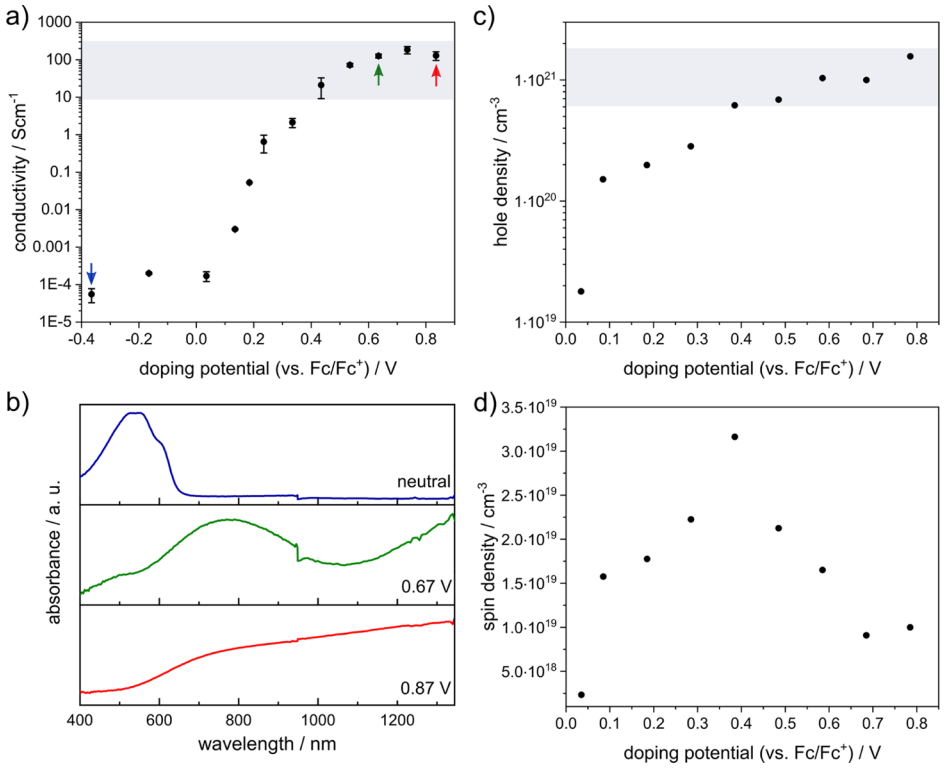

Figure 2. *Ex situ*-measured solid-state conductivities (a) and corresponding UV−vis−NIR spectra at three selected doping potentials (b) of electrochemically doped P3HT films on 4-line electrodes (an extended UV−vis−NIR spectrum up to 2200 nm can be found in Figure S8). (c) Calculation of the corresponding hole density is based on the evaluation of the injected charge during the potentiostatic doping process performed on Au-coated Kapton. (d) Spin densities calculated from EPR measurements from potentiostatically doped films on Au-coated Kapton.

species, which might be because of the high molecular weight and polydispersity of the P3HT that we used (M_n = 46.6 kg mol^{-1}, PDI = 2.4).

The obtained conductance change (Figure 1c black) appears in a sigmoidal shape starting from a region of lower conductance for P3HT in its neutral state, where conductance remains low until the onset of the cyclic voltammogram is reached. The emerging doping process is accompanied by a strong increase in the conductance until a plateau-like region is entered at an oxidation potential of ∼0.3 V. This plateau of high conductance is fully developed when potentials of 0.4 V are reached. By reversing the potential sweep direction, the film can once again be brought into the neutral state with low conductance proving the reversibility of the doping experiment (see Figure S3 for backward cycle of the conductance change).

As the absorption band evolution of the differently charged species implies, the plateau of highest conductance suggests the presence of differently charged species. Below 0.3 V—during the steep increase of conductance—there seem to be mainly neutral and polaron species present. The strong increase of the absorption at 1600 nm (which is around the beginning of the plateau at ∼0.3 V) further suggests the point where there is considerable formation of bipolarons, suggesting their importance in highly conducting states. This agrees with *in situ* EPR spectroscopy from Enengl *et al.*[51] Literature reports evidence that mixed valence states involving bipolarons tend to be highly conductive compared to mixed valence states containing only neutral and polaron species.[7] In view of the substantial conductance at potentials where bipolaron concentration should still be low, a conduction mechanism that is exclusively based on bipolarons[9,63] is therefore unlikely. We refer to Heinze *et al.* for further discussions of this topic.[12]

Interestingly, our data show the existence of the neutral species up to 0.8 V, implying a broad potential range where we seem to have mixed charge transport between neutral/polaron and polaron/bipolaron redox couples. These findings agree well with recent DFT-studies from Zozoulenko *et al.*, suggesting a coexistence of differently charged species over the whole applied potential range.[11]

2.2. *Ex Situ* Studies of Electrochemically Doped P3HT Films. *2.2.1. Ex Situ-Measured Solid-State Conductivities.* Although all previously presented experiments were performed *in situ* employing a dynamic potential sweep to investigate the oxidation (doping) behavior of the P3HT films on interdigitated electrodes, the following experiments were conducted using new tailor-made 4-line gold electrodes. These 4-line electrodes allow for the application of defined potentials to the polymer film by electrochemical doping in the electrochemical cell and can furthermore be used straightaway to measure reliable conductivities in the dry solid state. P3HT films were deposited by spin-coating onto the 4-line electrodes and then potentiostatically charged at defined oxidation potentials. During potentiostatic charging, the current was recorded until it approached zero, indicating a completed oxidation process. Respective current−time graphs are provided in Figure S4. The electrochemically doped films were then removed from the electrolyte, and solid-state conductivity measurements were conducted.

An important feature of our procedure is that the entire experiment is performed under the inert conditions of a glovebox with short times between potentiostatic charging in

https://dx.doi.org/10.1021/acs.chemmater.0c01293
Chem. Mater. 2020, 32, 6003−6013

the electrochemical cell and measurement of the conductivity in solid state. This setup excludes harmful influences of humidity on electronic conductivity that occur when moisture from the air comes in contact with highly doped polymer films.[64] The line-based electrode geometry helps to reduce contact issues especially in samples with low conductivities. Reference measurements in a traditional 4-point probe geometry gave similar conductivity values.

Because maintaining the counterions from the electrolyte inside the film is crucial to securing the obtained highly doped state, the samples are not washed after doping and removal from the electrochemical cell. This procedure does not impact the electronic conductivity measurements because even when ions from the electrolyte are still on the sample, electronic conductivity is dominant.[64]

Washing of the doped samples turned out to reduce the conductivity by at least 1 order of magnitude in our experimental procedure. This can be explained by the fact that the counterions are washed away which leads to dedoping and hence less charge carriers in the highly doped samples. This might be the reason for only low conductivities of electrochemically doped P3HT and polythiophene films reported in the literature so far.[65,66]

Figure 2a presents the results of the *ex situ*-measured solid-state conductivity measurements as function of the applied electrochemical doping potential. The conductivity data clearly show a sigmoidal shape with an extended plateau of high conductivity from 0.4 to 0.85 V. This trend is comparable to the obtained conductance change in the *in situ* experiment given in Figure 2c. The measured conductivity values are independent of the channel length of the 4-line electrodes and independent from the film thickness of the deposited P3HT film (see Figure S5).

At low doping potentials, before reaching a doping potential of ∼0.05 V, the conductivities are rather low in the range of 10^{-4} S cm^{-1}. Above 0.05 V, a strong increase of conductivity by over 6 orders of magnitude is observed. The conductivity becomes rather constant at doping potentials above 0.4 V with conductivities ranging from above 10 up to 220 S cm^{-1}. Maximum conductivities of 224 S cm^{-1} are reached which are impressive values when compared to literature of chemically doped samples.

For the system P3HT/F_4TCNQ, published conductivities peak in the region of 48 S cm^{-1} for films doped through the vapor phase.[67] $FeCl_3$ doping gave high conductivities of up to 63 S cm^{-1} for blade-coated P3HT films.[16] Only strongly oriented films of P3HT provided conductivities in the same order of magnitude with measured values of 250 and 570 S cm^{-1} by exploiting techniques like small-molecule epitaxy[68] or high-temperature rubbing,[16] respectively. Also Müller and co-workers suggested that high conductivities are achievable only with high crystallinities and order.[16,32,67] Our reported high conductivities over the broad doping potential range are however obtained by a simple spin-coating procedure from toluene solution. The rather disordered nature of the films is proven by atomic force microscopy (AFM) (Figure S6) and absorption spectroscopy in the neutral state; see discussion below. The influence of many amorphous regions in regioregular P3HT films on the resulting conductivity is further evidenced by measurements on completely amorphous films of regiorandom P3HT (see Figure S7). These experiments delivered conductivities of up to 10 S cm^{-1}, which is 2 orders of magnitude higher than reported for chemically doped regiorandom P3HT films by Müller *et al.*[32]

The conductivities of the regiorandom P3HT films are overall 1 order of magnitude lower compared to the regioregular P3HT films, Figure S7, which fits to findings in literature.[32] For completely amorphous films, these values are still very impressive and underline the success of our *ex situ* doping strategy, implying that high crystallinity with perfect long-range orientation is not a prerequisite to achieving high conductivities in semicrystalline polymer films. Although a certain degree of crystallinity seems favorable, good short-range order with efficient $\pi-\pi$ aggregation is of higher importance regarding electronic properties. This goes more in line with predictions from theoretical studies from Zozoulenko and co-workers who show that only efficient $\pi-\pi$ aggregation with a network of percolation paths seems to be essential for good electric performance.[33−35]

Possibly, the rather low crystallinity of the films might be also favorable for incorporation and securing counterions to stabilize the doped states.[37] Counterion incorporation has also strong impact on the film morphology because upon electrochemical doping, the counterions also take solvent molecules with them into the films.[30,37] This process is always accompanied by swelling of the entire polymer film.[55] The higher the doping potential the more ions need to be incorporated into the film to counterbalance the (bi)polarons in the film and the more dominant swelling effects become therefore. Furthermore large amounts of counterion incorporation in the charged polymer films can influence the charge transport in a negative way *via* the so-called Coulomb scattering.[32] The Coulomb potential of a counterion in this case can act as a trap for charge carriers in its close distance leading to weaker electronic properties.[69]

In this context, our finding of a conductivity plateau in the potential region from 0.4 to 0.8 V (highlighted area in gray in Figure 2a) is even more significant. Our method allows to obtain high conductivities already at low doping levels where the counterion incorporation and swelling should still be low and less destructive for the film morphology than using high potentials and high doping levels. In the literature, it has also been shown that the tuning of doping levels is extremely important to optimize the thermoelectric performance in CP materials.[50]

2.2.2. Discussion of Nature of Charged Species in the Highly Conducting Films. To characterize the highly conducting states further, *ex situ* UV−vis−NIR (on 4-line gold substrates) and EPR spectra (on gold-coated Kapton foil substrates) were recorded in the solid state. The absorption spectra in Figure 2 show a neutral P3HT film and two films after electrochemical doping: one at the beginning of the conductivity plateau region (0.67 V) and one at the highest doping level (0.87 V). The spectrum of the neutral P3HT film (Figure 2b, blue) shows one characteristic broad band at around 540 nm with a weak shoulder at 610 nm, suggesting rather low crystallinity similar to the *in situ* measurements.[17]

The spectrum obtained after doping at 0.67 V (Figure 2b, green) shows the presence of the neutral species at 540 nm, a broad band at 780 nm, and a broader signal at 1200 nm and higher. The spectrum of the film doped at 0.87 V has no evidence of the neutral band but shows a very broad absorption over the whole wavelength range above 600 nm. When overlaying these spectra with the *in situ* spectra from *in situ* spectroelectrochemistry, one can deduce that films doped

https://dx.doi.org/10.1021/acs.chemmater.0c01293
Chem. Mater. 2020, 32, 6003−6013

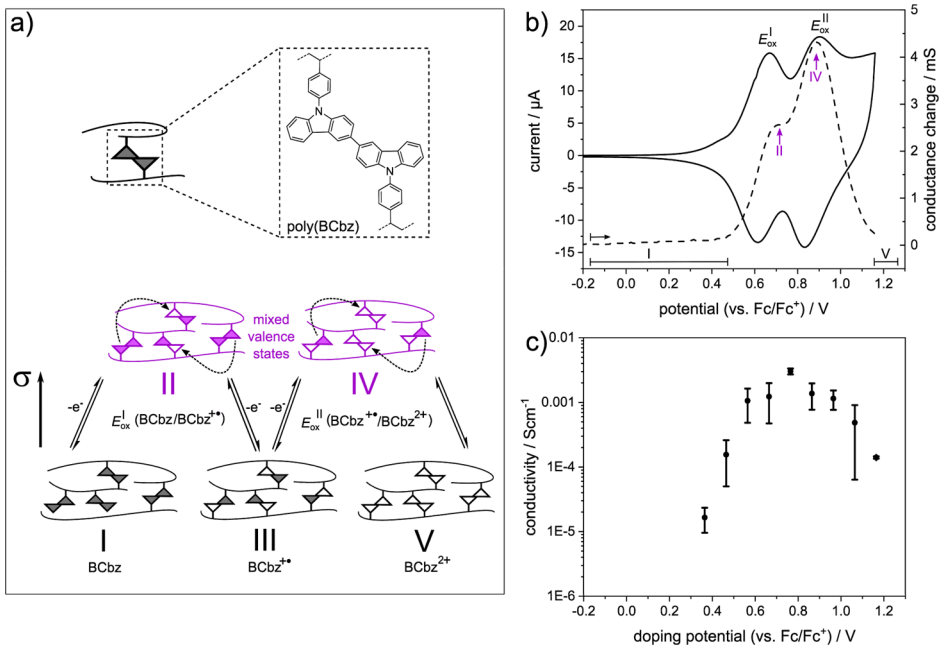

Figure 3. (a) Model of the chemical structure of a poly(BCbz) redox polymer film together with a sketch of mixed valence conductivity. (b) *In situ* conductance measurement (dotted black line, right axis, forward scan) with underlying cyclic voltammogram (solid black line, left axis) of poly(BCbz) measured in $TBAPF_6$/MeCN 0.1 M at 20 mV s^{-1} on an interdigitated Pt electrode. (c) Results of *ex situ*-measured solid-state conductivities of potentiostatically doped poly(BCbz) films on 4-line gold electrodes.

at 0.67 V contain polarons, bipolarons, and a certain amount of neutral species, while the 0.87 V doped film seems to contain essentially just polarons and bipolarons.

All observed bands are in accordance with the detected bands in the *in situ* experiments, leading to the conclusion that the doped states obtained upon electrochemical doping are stable in the solid state. It should be highlighted that mixed charged states containing neutral, polaron, and bipolaron could be successfully transferred from solution to the solid state. This is in stark contrast to earlier reports in the literature.[65] We have to stress that keeping the samples in the doped states is absolutely necessary, that means, washing and humidity should be avoided.

The discussion of the nature of the generated doped states can be extended by taking the charge carrier density into account; in this case, the hole density in Figure 2c. The injected charge during the electrochemical doping process of P3HT films on gold-coated Kapton substrates was extracted by integrating the area under the recorded current−time graphs (see Figure S9 for current−time graphs). The evolution of the hole density in dependence of the doping potential follows the expected trend with a constant increase of injected charge from low to high doping potentials. The highest charge carrier density achieved by our doping technique is in the order of 10^{21} holes per cm^3 which is comparable to the maximum hole densities presented for P3HT films in the literature, proving the reliability of our approach.[39,40,65]

The potentiostatically doped films on Kapton were further studied by EPR spectroscopy to track the dependence of the polaron concentration as a function of applied doping potential. This is possible because the ions which are integrated for charge compensation are EPR silent, so that purely, the P3HT doping can be followed. Experimentally, the films had to be cut and sealed in an EPR tube under inert conditions and subsequently investigated by means of EPR spectroscopy. The resulting spectra are displayed in Figure S10. There was no observable dependence of *g*-factor and linewidth on the orientation of the film with respect to the applied magnetic field, further suggesting the amorphous nature of the sample (Figure S11). At doping potentials below ∼0 V, that means, in the neutral state, no EPR signal can be detected because no unpaired electrons are present in the films.

First, EPR spectra could be obtained above ∼0 V which suggests the creation of polarons on the P3HT chains. The extracted change of the *g*-factor (Figure S10) with doping potential is small but significant, whereas the linewidth (Figure S10) shows a considerable increase. The linewidth increase can be interpreted as increased lifetime broadening because of (dipolar) interactions between polarons.

The double integral of the EPR spectrum is proportional to the number of spins and can be used to investigate the creation and conversion of polarons in P3HT in more depth. Figure 2d shows the spin density as a function of the doping potential.

The total amount of spins in Figure 2d shows a strong increase beyond 0 V and displays a maximum at doping potentials of ∼0.4 V. Increasing the doping potential above 0.4 V leads to a decrease of the total amount of spins. This is consistent with EPR-active polaronic states turning into EPR-silent bipolaronic charge carriers at higher doping levels, and we interpret our results in this manner.[51,66,70] However, a significant amount of spins and therefore polarons remain in the system even for the highest doping potential which means that polarons are present over the doping potential range from 0.1 to 0.8 V. The direct comparison with *in situ* EPR spectroelectrochemistry shows identical trends, suggesting that also the EPR measurements qualitatively prove that all *in situ* electrochemically doped species can in principle be transferred to the solid state.[51] It should be noted that doped samples for quantitative EPR measurements are highly sensitive and the

https://dx.doi.org/10.1021/acs.chemmater.0c01293
Chem. Mater. 2020, 32, 6003−6013

sample preparation, involving cutting and sealing of the samples into a tube, can lead to loss of charge carriers and hence an underestimation of the total amount of spins in the EPR. This can explain the discrepancy of 1 order of magnitude between injected charge carriers (measured from potentiostatic measurements in the electrochemical cell) and detected spins in the EPR measurements (measured *ex situ*).

In conclusion, our experimental evidence with conductivity, UV−vis−NIR, and EPR spectra as a function of the doping potential in the solid state supports a coexistence of at least two different redox species over the plateau of high conductivity that depending on the doping potential leans more toward polarons or bipolarons.

From the data, it is also possible to calculate the amount of thiophene-repeating units and the resulting charge per repeating unit. Regarding an intermediate doping potential of 0.4 V with the highest amount of spins, ∼0.15 charges per thiophene unit can be calculated. This corresponds roughly to one charge per five to six thiophene units, which correlates to the established picture of a polaron in P3HT. For the highest doping potential of 0.8 V, about 0.39 charges per thiophene unit can be obtained. This is close to two charges per five thiophene units, which could be explained by bipolaronic species. At these highest doping states, a maximum doping level of around 40% can be deduced (see conductivity as function of doping level in Figure S12).[51]

2.2.3. Comparison to Pure Redox Polymer Systems with Mixed Valence Conductivity. To set the presented results on electrochemically doped P3HT films in a wider context, the doping behavior of a more localized redox polymer system was examined. The idea was to demonstrate the conductivity behavior for a polymer system that shows pure intermolecular hopping transport because of localized redox centers. As redox centers, we chose bis(phenylcarbazole) which can be reversibly transferred from a neutral *via* a radical cation into a dication species; this is analogous to tetraphenylbenzidine species.[8,52]

For this purpose, the redox polymer poly(vinylphenylcarbazole) (PVPhCbz) was spin-coated from solution and transferred into an electrochemical three-electrode setup. Upon oxidation, the carbazole-active pendants generate dimeric bis(phenylcarbazole) (poly(BCbz)) units (Figure S13 for mechanism). This dimerization behavior simultaneously leads to a crosslinking of the entire polymer film, whereas the cross-link points are the redox-active BCbz units (Figure 3a). The procedure is motivated by our earlier research on triphenylamine-bearing polymers which can be easily dimerized by electrochemical oxidation into dimeric redox species based on tetraphenylbenzidine units.[8,52,71,72]

The created BCbz units are electroactive and can undergo a twofold oxidation from neutral to $BCbz^{\bullet+}$ radical cation into the $BCbz^{2+}$ dication state. The cyclic voltammogram of an electrochemically cross-linked PVPhCbz film—hereafter referred to as poly(BCbz)—(Figure 3b solid black) is therefore characterized by two chemically reversible peaks with half-wave potentials of 0.63 V for the neutral/radical cation couple ($BCbz/BCbz^{\bullet+}$) and 0.86 V for the radical cation/dication couple ($BCbz^{\bullet+}/BCbz^{2+}$), respectively.

The *in situ* conductance data of the poly(BCbz) film registered during the forward scan of the CV measurement (see Figure 3b dotted black line) gives a bell-shaped profile with a maximum at 0.89 V and a shoulder at 0.67 V; see Figure S14 for complete *in situ* conductance data with forward and backward scans. Both the peak maximum and the shoulder are located close to the half-wave potentials of the first and the second peak in the CV which can be explained by a mixed valence conductivity model in accordance to the literature.[5−7] Figure 3a shows a sketch of this model: in the neutral and fully oxidized state, no low conductance is obtained (states I and V), whereas the maxima of conductance are observed around the half-wave potentials when the highest amount of isoenergetic states between which hopping can take place is present (states II and IV). Interestingly, the first conductance regime, associated to hopping between neutral BCbz and the $BCbz^{\bullet+}$ radical cation species (state II) is lower in intensity with respect to the second conductance regime with $BCbz^{\bullet+}$ and $BCbz^{2+}$ species (state IV).

Because the redox waves for the first and second oxidation are very close to each other (no baseline separation), the pure presence of $BCbz^{\bullet+}$ radical cations (state III) is not visible. This would in principle also correspond to a low to nonconducting state. The two close oxidation potentials however lead to a merging of the conductance into a broader peak or "bell-shape" profile. In agreement with the literature, in this redox system, high conductance can only be realized when the electroactive units are present in different states of oxidation.[8,52]

The *ex situ*-doping approach used for P3HT was also pursued with the poly(BCbz) films. The solid-state conductivity as a function of different doping potentials of electrochemically doped poly(BCbz) films is presented in Figure 3c.

Above a threshold voltage of ∼0.34 V which corresponds to the onset potential of the oxidation in the *in situ* experiments, the conductivity strongly increases over 3 orders of magnitude. The highest measured conductivity of up to 3.4×10^{-3} S cm^{-1} is achieved at a doping potential of 0.75 V. A further increase of the doping potential leads to a decrease of the conductivity values as expected from the *in situ* measurements. Poly(BCbz) films therefore feature a bell-shape conductivity trend, where highest conductivities are only detected in a very narrow potential window. While the conductivity is decreasing at high potentials, it is still higher than what would be expected from the *in situ* conductance profile in Figure 3b. The partial decrease of the conductivity in comparison to the *in situ* measurements (Figure 3b) might be explained by dedoping effects upon transferring the electrochemically generated doped state into the solid state. We observed that the counterions are leaving the polymer films significantly more compared to P3HT films when transferring the film from the electrolyte into the solid state. This phenomenon will be the subject of further studies and becomes particularly crucial when structural information is targeted, for example, by transmission electron microscopy.[25]

Taking these data into account, a model for charge transport in the P3HT films might be proposed: The plateau conductivity with very high conductivities over a broad doping range might be explained as a consequence of many underlying conductivity maxima. Because of different chain lengths in a conjugated and polydisperse polymer like P3HT, a distribution in effective conjugation lengths seems intuitive. One could say that the P3HT polymer consists of sections of different effective conjugation lengths which could themselves be regarded as extended, delocalized redox systems varying in length. These extended redox systems would then have only slightly different oxidation potentials: A superposition of these multiple oxidized states with mixed charged species could be a

https://dx.doi.org/10.1021/acs.chemmater.0c01293
Chem. Mater. 2020, 32, 6003−6013

good explanation of the extended region of high conductivity, also taking into account the broad CV curves. The lack of clear isosbestic points in the *in situ* spectra underlines this statement.

3. CONCLUSIONS

In the presented work, we analyze the conductivity behavior of electrochemically doped P3HT films starting from dynamic *in situ* experiments in electrolyte. *In situ* conductance measurements show a sigmoidal conductance behavior with a plateau region of high conductance. *In situ* spectroelectrochemistry experiments conclude that at least two differently charged species are present over the entire doping potential range applied.

Proceeding from these results, solid-state conductivities of electrochemically doped P3HT films were recorded establishing a potentiostatic *ex situ*-doping approach. Reliable solid-state conductivities correlate with the *in situ* conductance change, confirming a successful transfer from *in situ* to *ex situ*. Maximum conductivities of up to 224 S cm^{-1} in highly doped states with maximum hole densities of 10^{21} holes per cm^3 for a P3HT film with low crystallinity are a highlight of this survey. Even completely amorphous films of regiorandom P3HT provide impressive conductivities, as high as 10 S cm^{-1}, questioning the importance of high crystallinity and perfect long-range order to obtain highly conducting films. The high conductivity follows theories suggesting that efficient $\pi-\pi$ aggregation containing only a short-range order is sufficient to achieve high bulk conductivities in CPs.

Our UV−vis−NIR and EPR data support the presence of mixed charged species suggested from the *in situ* experiments also for the solid state. Both first and second oxidized states (polaron and bipolaron) are coexisting even at the highest doping levels.

Finally, a comparison to a short and localized redox system from the family of redox polymers is pursued. Cross-linked films of poly(BCbz) show a bell-shaped *in situ* conductance profile with localized but merging conductance maxima. Similar trends can be extracted from the *ex situ* solid-state conductivity measurements with peak conductivities of up to 3.4×10^{-3} S cm^{-1} at intermediate doping levels.

Summarizing, the large versatility of electrochemical redox doping for both conjugated and redox polymers is demonstrated in a potentiostatic *ex situ* doping approach to generate highly CP films with tunable charge carrier densities that can be implemented in *ex situ* device applications. This study outlines the importance of identifying doping potential-dependent regions of conductivity for a successful implementation of CPs in organic electronic devices such as OECTs, batteries, or applications in the field of thermoelectrics. The role of intermolecular interactions and semicrystalline morphologies together with counterbalancing incorporated charges will be subject of further studies to increase conductivities.

4. EXPERIMENTAL SECTION

4.1. Materials. P3HT (regioregular: M_n = 46.6 kg mol^{-1}, PDI = 2.4, regioregularity of 95%; regiorandom: M_n = 15.9 kg mol^{-1}, PDI = 2.4) was purchased from Merck and used without further purification. Solvents (chloroform, toluene, and acetonitrile) were purchased from Sigma-Aldrich (p. a. grade) and used as received. Poly(vinylphenylcarbazole) (PVPhCbz, M_n = 2.3 kg mol^{-1}, PDI = 2.4) was synthesized according to literature procedures.[73−76]

4.2. Thin-Film Preparation. Thin films of P3HT with different thicknesses (10−80 nm) were processed from solutions in chloroform or toluene prepared in a glovebox at concentrations ranging from 3 to 8 g L^{-1}. All solutions were stirred overnight at elevated temperatures (40 °C for chloroform and 60 °C for toluene) to ensure complete dissolution. Films were spin-coated on precleaned substrates (subsequent ultrasonication in acetone and isopropanol) in a dry nitrogen atmosphere.

4.3. *In Situ* Conductance Measurements. For *in situ* conductance experiments, films of P3HT (thickness 30 nm) were spin-coated ($CHCl_3$, 3 g L^{-1}, 2500 rpm for 120 s, 5000 rpm for 15 s) on interdigitated platinum electrodes on glass substrates with a gap distance of 5 μm. Measurements were performed in an electrochemically gated transistor setup under argon atmosphere using a scan rate of 10 mV s^{-1} and 0.1 M tetra-*n*-butylammonium hexafluorophosphate ($TBAPF_6$, electrochemical grade, Sigma-Aldrich) in acetonitrile (MeCN) as the electrolyte. An additional bias of 10 mV was applied between the individual combs of the interdigitated electrode leading to a measured current that is converted into the conductance at a certain potential. All potentials were referenced against the redox couple Fc/Fc^+, added as the internal standard (after the measurement). The experiments were conducted by a commercial solution using a Metrohm PGSTAT101 potentiostat and a DropSens μSTAT400 as the second potentiostat, connected to two resistors (Heka) to separate the signals in order to allow simultaneous measurement of CV and *in situ* conductance. Because background currents cannot be neglected in this configuration, we focus on discussing conductance trends and not absolute values in this study. Therefore, *in situ* conductance data are given as conductance changes related to the conductance of the material in the neutral state.

4.4. 4-Line Probe Conductivity. Custom-made 4-line gold electrodes with a channel width of 1 cm and a channel length of 100 μm were evaporated on glass substrates and subsequently coated by spin coating from P3HT solutions (toluene, 3 g L^{-1}, 2000 rpm for 120 s, 5000 rpm for 15 s, and thickness 10 nm). The individual samples were electrochemically doped by potentiostatically charging in a three-electrode setup in standard electrolyte ($TBAPF_6$/MeCN 0.1 M) controlled by a Metrohm PGSTAT101 potentiostat. Doped samples were removed from the electrochemical setup, and solid-state conductivity measurements were conducted by a Keithley 2636 system source meter, operated by a self-written LabView program. The entire procedure was performed under inert conditions.

4.5. *In Situ* Spectroelectrochemical Measurements. The spectroelectrochemical experiments were performed on the same electrode geometry as used for the *in situ* conductance measurements. Films of P3HT were processed *via* spin coating ($CHCl_3$, 5 g L^{-1}, 1500 rpm for 120 s, 5000 rpm for 15 s, and thickness 50 nm) on interdigitated platinum electrodes on glass substrates. To allow for the detection of UV−vis−NIR data, the electrochemical cell ($TBAPF_6$/MeCN 0.1 M at 10 mV s^{-1}) was positioned in the beam path and the electrochemical setup was connected to a spectrometer *via* optical fibers. The *in situ* absorption spectra were recorded by a modular Zeiss spectrometer system (diode array) equipped with MCS611 2.2 and MCS621visII detectors and a CLH600 halogen lamp.

4.6. EPR Spectroscopy. Samples for EPR spectroscopy were prepared on custom-made gold coated Kapton foil (500 HN, DuPont) substrates. Films of P3HT were spin-coated ($CHCl_3$, 8 g L^{-1}, 1250 rpm for 120 s, 5000 rpm for 15 s, and thickness 80 nm) on the foil substrates and electrochemically doped in a three-electrode setup using a Metrohm PGSTAT101 potentiostat and standard electrolyte ($TBAPF_6$/MeCN 0.1 M) under argon atmosphere. Subsequently, films were transferred into EPR tubes (under inert conditions) and analyzed in the EPR spectrometer. EPR measurements were performed on a Bruker EMX X-Band spectrometer in a Bruker ER4102ST cavity. For all measurements, the microwave frequency was ∼9.47 GHz and the microwave power 5 mW. The magnetic field was modulated at 100 kHz with 1 Gauss amplitude. The measured spectra were fitted using the EasySpin package for MATLAB.[77] After obtaining the fit parameters (*g*-value, linewidth), the simulated spectra were doubly integrated to obtain the relative

https://dx.doi.org/10.1021/acs.chemmater.0c01293
Chem. Mater. 2020, 32, 6003−6013

numbers of spins. To obtain the absolute numbers of spins, the double integrals were compared to a calibration curve previously obtained from a concentration series of the 2,2-diphenyl-1-picrylhydrazyl (DPPH) radical.

■ ASSOCIATED CONTENT

Supporting Information

The Supporting Information is available free of charge at https://pubs.acs.org/doi/10.1021/acs.chemmater.0c01293.

Further *in situ* spectroelectrochemical data and conductivity for RR and regiorandom P3HT as well as PVPhCbz, EPR-data, and AFM morphology (PDF)

■ AUTHOR INFORMATION

Corresponding Author

Sabine Ludwigs − *IPOC—Functional Polymers, Institute of Polymer Chemistry, University of Stuttgart, 70569 Stuttgart, Germany*; orcid.org/0000-0002-6717-8538; Email: sabine.ludwigs@ipoc.uni-stuttgart.de

Authors

David Neusser − *IPOC—Functional Polymers, Institute of Polymer Chemistry, University of Stuttgart, 70569 Stuttgart, Germany*

Claudia Malacrida − *IPOC—Functional Polymers, Institute of Polymer Chemistry, University of Stuttgart, 70569 Stuttgart, Germany*

Michal Kern − *Institute of Physical Chemistry, University of Stuttgart, 70569 Stuttgart, Germany*

Yannic M. Gross − *IPOC—Functional Polymers, Institute of Polymer Chemistry, University of Stuttgart, 70569 Stuttgart, Germany*

Joris van Slageren − *Institute of Physical Chemistry, University of Stuttgart, 70569 Stuttgart, Germany*

Complete contact information is available at: https://pubs.acs.org/10.1021/acs.chemmater.0c01293

Notes

The authors declare no competing financial interest.

■ ACKNOWLEDGMENTS

The authors thank the IQST at the University of Stuttgart for funding through the Carl Zeiss Foundation, and the Deutsche Forschungsgemeinschaft (DFG) for funding within the CRC-1333 (project 358283783). The project was supported by Philipp Sliskovic and Dr. Klaus Dirnberger regarding the synthesis of PVPhCBz which is highly acknowledged.

■ REFERENCES

(1) Swager, T. M. 50th Anniversary Perspective: Conducting/Semiconducting Conjugated Polymers. A Personal Perspective on the Past and the Future. *Macromolecules* **2017**, *50*, 4867−4886.

(2) *P3HT Revisited—From Molecular Scale to Solar Cell Devices*; Ludwigs, S., Ed.; Springer Berlin Heidelberg: Berlin, Heidelberg, 2014; Vol. *265*.

(3) Reynolds, J. R.; Thompson, B. C.; Skotheim, T. A. *Handbook of Conducting Polymers*, 4th ed.; CRC Press: Boca Raton, 2019.

(4) Gracia, R.; Mecerreyes, D. Polymers with Redox Properties: Materials for Batteries, Biosensors and more. *Polym. Chem.* **2013**, *4*, 2206−2214.

(5) Salinas, G.; Frontana-Uribe, B. A. Analysis of Conjugated Polymers Conductivity by in situ Electrochemical-Conductance Method. *ChemElectroChem* **2019**, *6*, 4105−4117.

(6) Ofer, D.; Crooks, R. M.; Wrighton, M. S. Potential Dependence of the Conductivity of Highly Oxidized Olythiophenes, Polypyrroles, and Polyaniline: Finite Windows of High Conductivity. *J. Am. Chem. Soc.* **1990**, *112*, 7869−7879.

(7) Zotti, G.; Schiavon, G. Spin and Spinless Conductivity in Polypyrrole. Evidence for mixed-valence Conduction. *Chem. Mater.* **1991**, *3*, 62−65.

(8) Yurchenko, O.; Heinze, J.; Ludwigs, S. Electrochemically Induced Formation of Independent Conductivity Regimes in Polymeric Tetraphenylbenzidine Systems. *Chemphyschem* **2010**, *11*, 1637−1640.

(9) Brédas, J. L.; Street, G. B. Polarons, Bipolarons, and Solitons in Conducting Polymers. *Acc. Chem. Res.* **1985**, *18*, 309−315.

(10) Salzner, U. Electronic Structure of Conducting Organic Polymers: Insights from time-dependent Density Functional Theory. *Wiley Interdiscip. Rev.: Comput. Mol. Sci.* **2014**, *4*, 601−622.

(11) Zozoulenko, I.; Singh, A.; Singh, S. K.; Gueskine, V.; Crispin, X.; Berggren, M. Polarons, Bipolarons, And Absorption Spectroscopy of PEDOT. *ACS Appl. Polym. Mater.* **2019**, *1*, 83−94.

(12) Heinze, J.; Frontana-Uribe, B. A.; Ludwigs, S. Electrochemistry of Conducting Polymers-Persistent Models and new Concepts. *Chem. Rev.* **2010**, *110*, 4724−4771.

(13) Chidsey, C. E. D.; Murray, R. W. Redox Capacity and Direct Current Electron Conductivity in Electroactive Materials. *J. Phys. Chem.* **1986**, *90*, 1479−1484.

(14) Kaufman, F. B.; Schroeder, A. H.; Engler, E. M.; Kramer, S. R.; Chambers, J. Q. Ion and Electron Transport in Stable, Electroactive Tetrathiafulvalene Polymer Coated Electrodes. *J. Am. Chem. Soc.* **1980**, *102*, 483−488.

(15) Heinze, J.; Tschuncky, P. *The Oligomer Approach*; Müllen, K., Wegner, G., Eds.; VCH-Wiley: Weinheim, 1998.

(16) Vijayakumar, V.; Zhong, Y.; Untilova, V.; Bahri, M.; Herrmann, L.; Biniek, L.; Leclerc, N.; Brinkmann, M. Bringing Conducting Polymers to High Order: Toward Conductivities beyond 10^5 S cm $^{-1}$ and Thermoelectric Power Factors of 2 mW m $^{-1}$ K $^{-2}$. *Adv. Energy Mater.* **2019**, *9*, 1900266.

(17) Hartmann, L.; Tremel, K.; Uttiya, S.; Crossland, E.; Ludwigs, S.; Kayunkid, N.; Vergnat, C.; Brinkmann, M. 2D Versus 3D Crystalline Order in Thin Films of Regioregular Poly(3-hexylthiophene) Oriented by Mechanical Rubbing and Epitaxy. *Adv. Funct. Mater.* **2011**, *21*, 4047−4057.

(18) Tremel, K. Morphology of P3HT in Thin Films in Relation to Optical and Electrical Properties. In *P3HT Revisited—From Molecular Scale to Solar Cell Devices*; Ludwigs, S., Ed.; Springer Berlin Heidelberg: Berlin, Heidelberg, 2014; Vol. *265*.

(19) Crossland, E. J. W.; Tremel, K.; Fischer, F.; Rahimi, K.; Reiter, G.; Steiner, U.; Ludwigs, S. Anisotropic Charge Transport in Spherulitic Poly(3-hexylthiophene) Films. *Adv. Mater.* **2012**, *24*, 839−844.

(20) Meredig, B.; Salleo, A.; Gee, R. Ordering of Poly(3-hexylthiophene) Nanocrystallites on the Basis of Substrate Surface Energy. *ACS Nano* **2009**, *3*, 2881−2886.

(21) Kiefer, D.; Kroon, R.; Hofmann, A. I.; Sun, H.; Liu, X.; Giovannitti, A.; Stegerer, D.; Cano, A.; Hynynen, J.; Yu, L.; et al. Double Doping of Conjugated Polymers with Monomer Molecular Dopants. *Nat. Mater.* **2019**, *18*, 149−155.

(22) Jacobs, I. E.; Aasen, E. W.; Oliveira, J. L.; Fonseca, T. N.; Roehling, J. D.; Li, J.; Zhang, G.; Augustine, M. P.; Mascal, M.; Moulé, A. J. Comparison of Solution-mixed and Sequentially Processed P3HT:F4TCNQ Films: Effect of Doping-induced Aggregation on Film Morphology. *J. Mater. Chem. C* **2016**, *4*, 3454−3466.

(23) Reinold, P.; Bruchlos, K.; Ludwigs, S. Simultaneous Doping and Crosslinking of Polythiophene Films. *Polym. Chem.* **2017**, *8*, 7351−7359.

(24) Jacobs, I. E.; Moulé, A. J. Controlling Molecular Doping in Organic Semiconductors. *Adv. Mater.* **2017**, *29*, 1703063.

(25) Gross, Y. M.; Trefz, D.; Dingler, C.; Bauer, D.; Vijayakumar, V.; Untilova, V.; Biniek, L.; Brinkmann, M.; Ludwigs, S. From Isotropic

to Anisotropic Conductivities in P(NDI2OD-T 2) by (Electro-)Chemical Doping Strategies. *Chem. Mater.* **2019**, *31*, 3542−3555.
(26) Dingler, C.; Dirnberger, K.; Ludwigs, S. Semiconducting Polymer Spherulites-From Fundamentals to Polymer Electronics. *Macromol. Rapid Commun.* **2019**, *40*, 1800601.
(27) Kratochvil, B.; Long, R. Iron(III)-(II) couple in acetonitrile. Oxidation of thiocyanate by iron(III). *Anal. Chem.* **1970**, *42*, 43−46.
(28) Rainbolt, J. E.; Koech, P. K.; Polikarpov, E.; Swensen, J. S.; Cosimbescu, L.; Von Ruden, A.; Wang, L.; Sapochak, L. S.; Padmaperuma, A. B.; Gaspar, D. J. Synthesis and Characterization of P-type Conductivity Dopant 2-(3-(adamantan-1-yl)propyl)-3,5,6-trifluoro-7,7,8,8-tetracyanoquinodimethane. *J. Mater. Chem. C* **2013**, *1*, 1876−1884.
(29) Aubry, T. J.; Winchell, K. J.; Salamat, C. Z.; Basile, V. M.; Lindemuth, J. R.; Stauber, J. M.; Axtell, J. C.; Kubena, R. M.; Phan, M. D.; Bird, M. J.; Spokoyny, A. M.; Tolbert, S. H.; Schwartz, B. J. Tunable Dopants with Intrinsic Counterion Separation Reveal the Effects of Electron Affinity on Dopant Intercalation and Free Carrier Production in Sequentially Doped Conjugated Polymer Films. *Adv. Funct. Mater.* **2020**, *30*, 2001800.
(30) Bruchlos, K.; Trefz, D.; Hamidi-Sakr, A.; Brinkmann, M.; Heinze, J.; Ruff, A.; Ludwigs, S. Poly(3-hexylthiophene) Revisited − Influence of Film Deposition on the Electrochemical Behaviour and Energy Levels. *Electrochim. Acta* **2018**, *269*, 299−311.
(31) Cardona, C. M.; Li, W.; Kaifer, A. E.; Stockdale, D.; Bazan, G. C. Electrochemical Considerations for Determining Absolute Frontier Orbital Energy Levels of Conjugated Polymers for Solar Cell Applications. *Adv. Mater.* **2011**, *23*, 2367−2371.
(32) Hynynen, J.; Kiefer, D.; Yu, L.; Kroon, R.; Munir, R.; Amassian, A.; Kemerink, M.; Müller, C. Enhanced Electrical Conductivity of Molecularly p-Doped Poly(3-hexylthiophene) through Understanding the Correlation with Solid-State Order. *Macromolecules* **2017**, *50*, 8140−8148.
(33) Rolland, N.; Franco-Gonzalez, J. F.; Volpi, R.; Linares, M.; Zozoulenko, I. V. Understanding morphology-mobility dependence in PEDOT:Tos. *Phys. Rev. Mater.* **2018**, *2*, 045605.
(34) Noriega, R.; Rivnay, J.; Vandewal, K.; Koch, F. P. V.; Stingelin, N.; Smith, P.; Toney, M. F.; Salleo, A. A general Relationship Between Disorder, Aggregation and Charge Transport in Conjugated Polymers. *Nat. Mater.* **2013**, *12*, 1038−1044.
(35) Wang, S.; Fabiano, S.; Himmelberger, S.; Puzinas, S.; Crispin, X.; Salleo, A.; Berggren, M. Experimental Evidence that Short-range Intermolecular Aggregation is Sufficient for Efficient Charge Transport in Conjugated Polymers. *Proc. Natl. Acad. Sci. U.S.A.* **2015**, *112*, 10599−10604.
(36) Yuen, J. D.; Dhoot, A. S.; Namdas, E. B.; Coates, N. E.; Heeney, M.; McCulloch, I.; Moses, D.; Heeger, A. J. Electrochemical Doping in Electrolyte-Gated Polymer Transistors. *J. Am. Chem. Soc.* **2007**, *129*, 14367−14371.
(37) Rawlings, D.; Thomas, E. M.; Segalman, R. A.; Chabinyc, M. L. Controlling the Doping Mechanism in Poly(3-hexylthiophene) Thin-Film Transistors with Polymeric Ionic Liquid Dielectrics. *Chem. Mater.* **2019**, *31*, 8820−8829.
(38) Shomura, R.; Sugiyasu, K.; Yasuda, T.; Sato, A.; Takeuchi, M. Electrochemical Generation and Spectroscopic Characterization of Charge Carriers within Isolated Planar Polythiophene. *Macromolecules* **2012**, *45*, 3759−3771.
(39) Thomas, E. M.; Brady, M. A.; Nakayama, H.; Popere, B. C.; Segalman, R. A.; Chabinyc, M. L. X-Ray Scattering Reveals Ion-Induced Microstructural Changes During Electrochemical Gating of Poly(3-Hexylthiophene). *Adv. Funct. Mater.* **2018**, *28*, 1803687.
(40) Wang, S.; Ha, M.; Manno, M.; Frisbie, C. D.; Leighton, C. Hopping Transport and the Hall effect Near the Insulator-Metal Transition in Electrochemically Gated Poly(3-hexylthiophene) Transistors. *Nat. Commun.* **2012**, *3*, 1210.
(41) Glaudell, A. M.; Cochran, J. E.; Patel, S. N.; Chabinyc, M. L. Impact of the Doping Method on Conductivity and Thermopower in Semiconducting Polythiophenes. *Adv. Energy Mater.* **2015**, *5*, 1401072.
(42) Hamidi-Sakr, A.; Biniek, L.; Bantignies, J.-L.; Maurin, D.; Herrmann, L.; Leclerc, N.; Lévêque, P.; Vijayakumar, V.; Zimmermann, N.; Brinkmann, M. A Versatile Method to Fabricate Highly In-Plane Aligned Conducting Polymer Films with Anisotropic Charge Transport and Thermoelectric Properties: The Key Role of Alkyl Side Chain Layers on the Doping Mechanism. *Adv. Funct. Mater.* **2017**, *27*, 1700173.
(43) Zhang, Q.; Sun, Y.; Xu, W.; Zhu, D. What To Expect from Conducting Polymers on the Playground of Thermoelectricity: Lessons Learned from Four High-Mobility Polymeric Semiconductors. *Macromolecules* **2014**, *47*, 609−615.
(44) Laiho, A.; Herlogsson, L.; Forchheimer, R.; Crispin, X.; Berggren, M. Controlling the Dimensionality of Charge Transport in Organic Thin-Film Transistors. *Proc. Natl. Acad. Sci. U.S.A.* **2011**, *108*, 15069−15073.
(45) Zanettini, S.; Chaumy, G.; Chávez, P.; Leclerc, N.; Etrillard, C.; Leconte, B.; Chevrier, F.; Dayen, J.-F.; Doudin, B. High Conductivity Organic Thin Films for Spintronics: The Interface Resistance Bottleneck. *J. Phys.: Condens. Matter* **2015**, *27*, 462001.
(46) Sun, H.; Gerasimov, J.; Berggren, M.; Fabiano, S. N-Type Organic Electrochemical Transistors: Materials and Challenges. *J. Mater. Chem. C* **2018**, *6*, 11778−11784.
(47) Flagg, L. Q.; Giridharagopal, R.; Guo, J.; Ginger, D. S. Anion-Dependent Doping and Charge Transport in Organic Electrochemical Transistors. *Chem. Mater.* **2018**, *30*, 5380−5389.
(48) Toss, H.; Suspène, C.; Piro, B.; Yassar, A.; Crispin, X.; Kergoat, L.; Pham, M.-C.; Berggren, M. On the Mode of Operation in Electrolyte-Gated Thin Film Transistors Based on Different Substituted Polythiophenes. *Org. Electron.* **2014**, *15*, 2420−2427.
(49) Bubnova, O.; Berggren, M.; Crispin, X. Tuning the Thermoelectric Properties of Conducting Polymers in an Electrochemical Transistor. *J. Am. Chem. Soc.* **2012**, *134*, 16456−16459.
(50) Bubnova, O.; Khan, Z. U.; Malti, A.; Braun, S.; Fahlman, M.; Berggren, M.; Crispin, X. Optimization of the Thermoelectric Figure of Merit in the Conducting Polymer Poly(3,4-ethylenedioxythiophene). *Nat. Mater.* **2011**, *10*, 429−433.
(51) Enengl, C.; Enengl, S.; Pluczyk, S.; Havlicek, M.; Lapkowski, M.; Neugebauer, H.; Ehrenfreund, E. Doping-Induced Absorption Bands in P3HT: Polarons and Bipolarons. *Chemphyschem* **2016**, *17*, 3836−3844.
(52) Yurchenko, O.; Freytag, D.; Zur Borg, L.; Zentel, R.; Heinze, J.; Ludwigs, S. Electrochemically Induced Reversible and Irreversible Coupling of Triarylamines. *J. Phys. Chem. B* **2012**, *116*, 30−39.
(53) Krische, B.; Zagorska, M. Overoxidation in Conducting Polymers. *Synth. Met.* **1989**, *28*, 257−262.
(54) Wieland, M.; Malacrida, C.; Yu, Q.; Schlewitz, C.; Scapinello, L.; Penoni, A.; Ludwigs, S. Conductance and Spectroscopic Mapping of EDOT Polymer Films upon Electrochemical Doping. *Flexible Printed Electron.* **2020**, *5*, 014016.
(55) Scholes, D. T.; Yee, P. Y.; Lindemuth, J. R.; Kang, H.; Onorato, J.; Ghosh, R.; Luscombe, C. K.; Spano, F. C.; Tolbert, S. H.; Schwartz, B. J. The Effects of Crystallinity on Charge Transport and the Structure of Sequentially Processed F 4 TCNQ-Doped Conjugated Polymer Films. *Adv. Funct. Mater.* **2017**, *27*, 1702654.
(56) Yamagata, H.; Spano, F. C. Interplay Between Intrachain and Interchain Interactions in Semiconducting Polymer Assemblies: The HJ-Aggregate Model. *J. Chem. Phys.* **2012**, *136*, 184901.
(57) Skompska, M.; Szkurłat, A. The Influence of the Structural Defects and Microscopic Aggregation of Poly(3-alkylthiophenes) on Electrochemical and Optical Properties of the Polymer Films: Discussion of an Origin of Redox Peaks in the Cyclic Voltammograms. *Electrochim. Acta* **2001**, *46*, 4007−4015.
(58) Havinga, E. E.; Mutsaers, C. M. J.; Jenneskens, L. W. Absorption Properties of Alkoxy-Substituted Thienylene−Vinylene Oligomers as a Function of the Doping Level. *Chem. Mater.* **1996**, *8*, 769−776.
(59) Yamamoto, J.; Furukawa, Y. Electronic and Vibrational Spectra of Positive Polarons and Bipolarons in Regioregular Poly(3-

https://dx.doi.org/10.1021/acs.chemmater.0c01293
Chem. Mater. 2020, 32, 6003−6013

hexylthiophene) Doped with Ferric Chloride. *J. Phys. Chem. B* **2015**, *119*, 4788−4794.
(60) van Haare, J. A. E. H.; Havinga, E. E.; van Dongen, J. L. J.; Janssen, R. A. J.; Cornil, J.; Brédas, J.-L. Redox States of Long Oligothiophenes: Two Polarons on a Single Chain. *Chem.—Eur. J.* **1998**, *4*, 1509−1522.
(61) Rana, D.; Donfack, P.; Jovanov, V.; Wagner, V.; Materny, A. Ultrafast Polaron-Pair Dynamics in a Poly(3-hexylthiophene-2,5-diyl) Device Influenced by a Static Electric Field: Insights into Electric-Field-Related Charge Loss. *Phys. Chem. Chem. Phys.* **2019**, *21*, 21236−21248.
(62) Baeuerle, P.; Segelbacher, U.; Maier, A.; Mehring, M. Electronic Structure of Mono- and Dimeric Cation Radicals in End-Capped Oligothiophenes. *J. Am. Chem. Soc.* **1993**, *115*, 10217−10223.
(63) Bredas, J. L. Bipolarons in Doped Conjugated Polymers: A Critical Comparison Between Theoretical Results and Experimental Data. *Mol. Cryst. Liq. Cryst.* **1985**, *118*, 49−56.
(64) Wieland, M.; Dingler, C.; Merkle, R.; Maier, J.; Ludwigs, S. Humidity-Controlled Water Uptake and Conductivities in Ion and Electron Mixed Conducting Polythiophene Films. *ACS Appl. Mater. Interfaces* **2020**, *12*, 6742−6751.
(65) Harris, J. K.; Neelamraju, B.; Ratcliff, E. L. Intersystem Subpopulation Charge Transfer and Conformational Relaxation Preceding in Situ Conductivity in Electrochemically Doped Poly(3-hexylthiophene) Electrodes. *Chem. Mater.* **2019**, *31*, 6870−6879.
(66) Kaneto, K.; Hayashi, S.; Ura, S.; Yoshino, K. ESR and Transport Studies in Electrochemically Doped Polythiophene Film. *J. Phys. Soc. Jpn.* **1985**, *54*, 1146−1153.
(67) Lim, E.; Peterson, K. A.; Su, G. M.; Chabinyc, M. L. Thermoelectric Properties of Poly(3-hexylthiophene) (P3HT) Doped with 2,3,5,6-Tetrafluoro-7,7,8,8-tetracyanoquinodimethane (F 4 TCNQ) by Vapor-Phase Infiltration. *Chem. Mater.* **2018**, *30*, 998−1010.
(68) Qu, S.; Yao, Q.; Wang, L.; Chen, Z.; Xu, K.; Zeng, H.; Shi, W.; Zhang, T.; Uher, C.; Chen, L. Highly Anisotropic P3HT Films with Enhanced Thermoelectric Performance via Organic Small Molecule Epitaxy. *NPG Asia Mater.* **2016**, *8*, No. e292.
(69) Zuo, G.; Li, Z.; Andersson, O.; Abdalla, H.; Wang, E.; Kemerink, M. Molecular Doping and Trap Filling in Organic Semiconductor Host−Guest Systems. *J. Phys. Chem. C* **2017**, *121*, 7767−7775.
(70) Volkov, A. V.; Singh, S. K.; Stavrinidou, E.; Gabrielsson, R.; Franco-Gonzalez, J. F.; Cruce, A.; Chen, W. M.; Simon, D. T.; Berggren, M.; Zozoulenko, I. V. Spectroelectrochemistry and Nature of Charge Carriers in Self-Doped Conducting Polymer. *Adv. Electron. Mater.* **2017**, *3*, 1700096.
(71) Blanchard, P.; Malacrida, C.; Cabanetos, C.; Roncali, J.; Ludwigs, S. Triphenylamine and some of its Derivatives as versatile Building Blocks for Organic Electronic Applications. *Polym. Int.* **2019**, *68*, 589−606.
(72) Malacrida, C.; Habibi, A. H.; Gámez-Valenzuela, S.; Lenko, I.; Marqués, P. S.; Labrunie, A.; Grolleau, J.; López Navarrete, J. T.; Ruiz Delgado, M. C.; Cabanetos, C.; et al. Impact of the Replacement of a Triphenylamine by a Diphenylmethylamine Unit on the Electrochemical Behavior of Pentaerythritol-Based Push-Pull Tetramers. *ChemElectroChem* **2019**, *6*, 4215−4228.
(73) Monnier, F.; Taillefer, M. Katalytische C-C-, C-N- und C-O-Ullmann-Kupplungen. *Angew. Chem.* **2009**, *121*, 7088−7105.
(74) McKeown, N. B.; Badriya, S.; Helliwell, M.; Shkunov, M. The Synthesis of Robust, Polymeric Hole-Transport Materials from Oligoarylamine Substituted Styrenes. *J. Mater. Chem.* **2007**, *17*, 2088−2094.
(75) Behl, M.; Hattemer, E.; Brehmer, M.; Zentel, R. Tailored Semiconducting Polymers: Living Radical Polymerization and NLO-Functionalization of Triphenylamines. *Macromol. Chem. Phys.* **2002**, *203*, 503−510.
(76) Shi, H.-p.; Xu, L.; Cheng, Y.; He, J.-y.; Dai, J.-x.; Xing, L.-w.; Chen, B.-q.; Fang, L. Experimental and Theoretical Study of three new Benzothiazole-fused Carbazole Derivatives. *Spectrochim. Acta, Part A* **2011**, *81*, 730−738.
(77) Stoll, S.; Schweiger, A. EasySpin, a Comprehensive Software Package for Spectral Simulation and Analysis in EPR. *J. Magn. Reson.* **2006**, *178*, 42−55.

https://dx.doi.org/10.1021/acs.chemmater.0c01293
Chem. Mater. 2020, 32, 6003−6013